14

Updating Scarce High Resolution Images with Time Series of Coarser Images: a Bayesian Data Fusion Solution

Dominique Fasbender[1], Valérie Obsomer[1,2],
Patrick Bogaert[1] and Pierre Defourny[1]
[1]*Dpt of Environmental Sciences and Land Use Planning, Université catholique de Louvain*
[2]*Institute of Tropical Medecine, Antwerpen*
Belgium

1. Introduction

As a consequence of the great variability between sensors, the characteristics of remotely sensed data widely differ with respect to spectral and spatial resolutions. Additionally to their respective technical characteristics and peculiarities, sensors also have different temporal frequencies of acquisition. Coarser sensors (e.g. SPOT VEGETATION or TERRA MODIS) have generally close to daily acquisition rates while high spatial resolution sensors (e.g. SPOT HRVIR or IKONOS) have lower acquisition rates. Cloud-free high resolution imagery may therefore not be available at the required period unlike coarser resolution images. On top of this, high resolution images are sometimes so highly priced that updating past high resolution images with recent coarse images can be cost effective. For these reasons, there is a real need for a sound theoretical framework that aims at merging information coming from two or more different sensors while taking explicitly into account the spatial resolution discrepancies between images. Typically, for cost effective applications, this could involve predicting a high resolution image by updating a past one with more recent but coarser images.

It is a common fact that remote sensors have different spatial resolution. This change of resolution is thus a typical issue in remote sensing applications. Depending on users' needs and the heterogenity of the study areas, different algorithms of fusion were proposed for the spatial enhancement of remotely sensed images. These include Brovey method (Pohl & van Genderen, 1998), Intensity-Hue-Saturation (IHS; Harrison & Jupp, 1990), Principal Component Analysis (PCA; Pohl & van Genderen, 1998), wavelet-based Multi-Resolution Analyses (MRA; Zhou et al., 1998; Garzelli & Nencini, 2005; Ranchin et al., 2003), High-Pass Filter (HPF; Chavez et al., 1991), generalized Laplacian methods (Aiazzi et al., 2002) and downscaling cokriging (Pardo-Iguzquiza et al., 2006), just to quote a few of them. Detailed reviews of the numerous available algorithms can be found in (Pohl & van Genderen, 1998; Chavez et al., 1991; Wang et al., 2005; Ballester et al., 2006 or Laporterie et al., 2005). Unfortunetely, most of these methods are devoted to the case of spatial enhancement of remotely sensed images only in the case of simultaneous images. In other words, the images to be fused are assumed to be taken at the same time but with different spectral bands and

Source: Sensor and Data Fusion, Book edited by: Dr. ir. Nada Milisavljević,
ISBN 978-3-902613-52-3, pp. 490, February 2009, I-Tech, Vienna, Austria

different spatial resolutions. It is therefore relevant to focus our attention on data fusion methods that typically enable us to account for several information sources in order to produce a single but improved image. Recently, a new Bayesian Data Fusion (BDF) framework was proposed in a general space-time prediction context by (Bogaert & Fasbender, 2007), with the aim of merging various kind of information sources that are all different but relevant for a same target variable. Though initially developed with stochastic space-time random fields applications in mind, the method proved to be efficient for remotely sensed applications as well (e.g. Fasbender et al., 2008b).
This chapter shows how the BDF approach can be used for the update of high resolution images with coarser images. In order to illustrate the general principle of the method, a synthetic case study was created from SPOT VEGETATION composite images (1km resolution) available at different dates. Spatially degraded 10km and 100km images are generated and used as coarse images. From the whole time-series of coarser images and only few of the initial images over time, it is then shown how BDF allows predicting the high resolution image at, say, date 2 by combining at the same time (i) the high-resolution image at a previous date 1, (ii) the coarser image at date 2, and (iii) the evolution of the coarser images between dates 1 and 2. Based on a quality assessment conducted by comparing the BDF-predicted images with the corresponding original 1 km images, it is shown that the method is able to provide both consistent results and improved images. Built on sound theoretical grounds, easy to implement and computationally fast, this method opens new avenues in the field of cost effective and efficient data fusion techniques for remotely sensed data.

2. Bayesian data fusion

Combining different sources of information into a single final result (i.e. data fusion) is a problem of general concern for a large panel of applications, that goes far beyond satellite imagery and encompasses a wide array of potential methods. Among them, Bayesian approaches have led to interesting applications with respect to various problems such as image surveillance (Jones et al. 2003), object recognition (Chung & Shen, 2000), object localization (Pinheiro & Lima, 2004), robotic (Moshiri et al., 2002), image processing (Rajan & Chaudhuri, 2002), classification of remote sensing images (Bruzzone et al., 2002) and environmental modelling (Wikle et al., 2001), just to quote few of them. The main advantage of a Bayesian approach is to set the problem of data fusion into a clear probabilistic framework. The present chapter relies on a general Bayesian Data Fusion approach in the context of spatial data (Bogaert & Fasbender, 2007). Its specific implementation will focus here on the problem of updating high resolution images with time series of coarser images.

2.1 General formulation

The basic concept of BDF as presented in (Bogaert & Fasbender, 2007) relies on the idea that variables of interest, denoted as vector $Z = (Z_1, \ldots Z_n)'$, cannot be directly observed. Instead, they are linked to the observable variables $Y_{i,j}$ through an error-like model, with

$$Y_{i,j} = g_{i,j}(Z_i) + E_{i,j} \tag{1}$$

where $g_{i,j}(.)$'s are functionals and E is a vector of random errors that are stochastically independent from Z. Assuming that the $E_{i,j}$'s of the random vector E are stochastically

independent, it is easy to obtain the conditional probability density function (pdf) of the vector of interest given the observed variables, with

$$f(z \mid y) \propto f_Z(z) \prod_{i=1}^{n} \prod_{j=1}^{p_i} f_{E_{i,j}}(y_{i,j} - g_{i,j}(z_i)) \tag{2}$$

where i corresponds to the channel number and p_i is the number of secondary information corresponding to the same Z_i (see Bogaert & Fasbender, 2007 for more details).
Using Bayes theorem again for $f_{E_{i,j}}(y_{i,j} - g_{i,j}(z_i)) = f(y_{i,j} \mid z_i)$, Eq. (2) becomes

$$f(z \mid y) \propto f_Z(z) \prod_{i=1}^{n} \prod_{j=1}^{p_i} \frac{f(z_i \mid y_{i,j})}{f(z_i)} \tag{3}$$

where $f(z_i)$ is the *a priori* distribution of Z_i. According to the information sources at hand, intermediate stages between Eq. (2) and Eq. (3) are possible as well (e.g. an expression mixing both $f_{E_{i,j}}(.)$ and $f(. \mid y_{i,j})$ distributions).

It is worth noting that this BDF framework has interesting similarities with other multi-sensor data fusion methods (see Mitchell, 2007 for more details). The advantage of the BDF framework over other existing multi-sensor data fusion methods is that it proposes a general formulation when accounting for several secondary information sources whatever the nature of these secondary information. Thanks to this, the range of applications that can be tackled by the BDF approach is wider and is far beyond the scope of the traditional multi-sensor fusion issue.

2.2 Specific assumptions

The previous section presented the general BDF framework but it is important here to choose some specific assumptions in order to tackle the issue of updating high resolution images. In this context, there are three sources of information available at each location, namely the high resolution image at date 1, the coarser image at date 1 and the coarser image at date 2. In our implementation, the following notations will be used :

- Z is the unknown multispectral reflectance values for the finer resolution pixel at date 2
- Y_H is the multispectral reflectance values for the finer resolution pixel at date 1
- Y_{L1} is the multispectral reflectance values for the coarser resolution pixel at date 1
- Y_{L2} is the multispectral reflectance values for the coarser resolution pixel at date 2

Let us first assume that the finer and the coarser images share the same spectral bands. In these conditions, several predictions methods for the unknown pixel Z, all based on these information sources, can be used. In this application, only two methods will be evaluated. The first one simply consists in using the coarser multispectral Y_{L2} has a raw estimate of the unknown pixel Z. Of course, although the image composed by the pixels Y_{L2} is smoother than the target high resolution image, the global fluctuations are accounted for in the smooth image. The unexplained part of the variabiliy is then the local fluctuations with a mean equal to zero for each of the spectral bands and a variance Σ_1 that can be estimated from the difference Y_H - Y_{L1} between high and coarser resolution images at date 1.

The second prediction considered here is based on the following High-Pass Filtering approach :

1. the high resolution image at date 1 is first decomposed into a lower frequencies image and a higher frequencies image using a Gaussian filter.
2. the higher frequencies image is then combined with the coarser image at date 2.

The resulting image has thus the advantages that details are provided by the high resolution image at date 1 whereas the global fluctuations are provided by the coarser image at date 2. The mean of this image is thus expected to be the same as the objective image and its variance Σ_2 can be estimated from the variance of Y_{L1} - Y_{L2}.

Now, assuming mutivariate Gaussian distribution for both secondary information sources as well as a non-informative *prior* distribution (i.e. constant distribution over the domain), the fused distribution is also a multivariate Gaussian distribution with a mean vector μ and a covariance matrix Σ given by

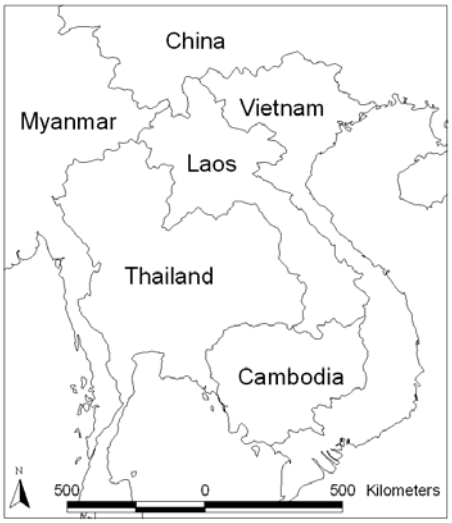

Fig. 1. Study site

$$\Sigma^{-1} = \Sigma_1^{-1} + \Sigma_2^{-1} \tag{4}$$

$$\mu = \Sigma(\Sigma_1^{-1}\mu_1 + \Sigma_2^{-1}\mu_2) \tag{5}$$

where μ_1 and μ_2 are respectively the two predictions decribed above. The value μ is thus a relevant candidate for the predition of the unknown finer resolution pixel Z.

Up to this point, it was assumed that finer and coarser images share the same spectral bands. However, this situation rarely occurs in real case applications. Fortunately, the generalization of the previous approaches is straightforward for non fully overlapping spectral bands. Indeed, one could easily generalize $Y_{L1} = Z + E$ into, e.g., $Y_{L1} = AZ + b + E$ with $b \in \mathbb{R}$ and $A \in \mathbb{R}^{n \times n}$ (i.e. the spectral bands of the coarser image are linked to the spectral bands of the target image through a translation vector b and a

scaling matrix A). Thanks to this, it is now theoretically possible to update high resolution images from a first sensor like e.g. SPOT HRVIR or IKONOS with time series of coarser images from a second sensor like e.g. TERRA MODIS or SPOT VEGETATION.

3. Demonstration case study

3.1 Simulated data

In this case study, coarser images were simulated from biweekly composite images based on real SPOT VEGETATION images with a spatial resolution of 1km. The original images were taken in the South-East Asia region (Fig. 1). Composite images were computed on a biweekly basis using the mean compositing method (Vancutsem et al., 2007). The covered period is 2004-2005 so that 50 images were available for this study. Fig. 2 shows this evolution for the year 2005. After a clouds screening, each original image was degraded at 10 km and 100km resolution by averaging all 1km pixels corresponding to the area. Resulting images were then resampled at 1km in order to match the original 1km spatial resolution (Fig. 3).

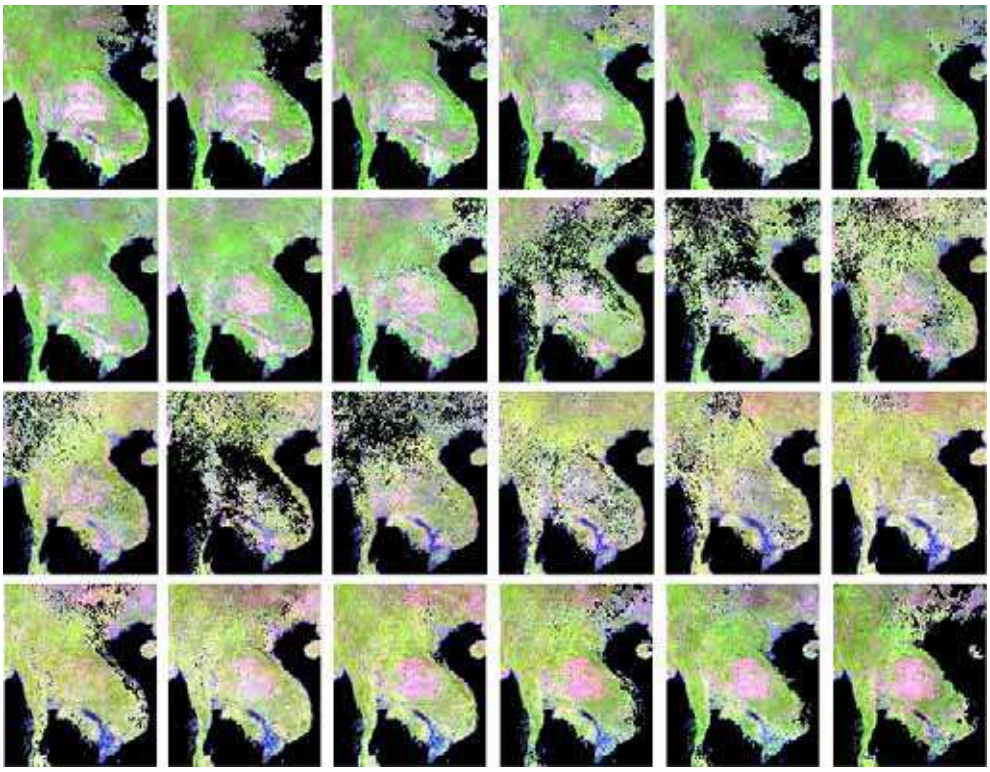

Fig. 2. Evolution of the original biweekly images at 1km resolution.

In the context of this chapter, original 1km images are assumed to be the finer images and blurry simulated ones are the coarser images. Furthermore, it is worth noting that spectral

bands of both the finer and the coarser images are the same so that the specific assumptions described in the previous section can be directly applied here without modifications.

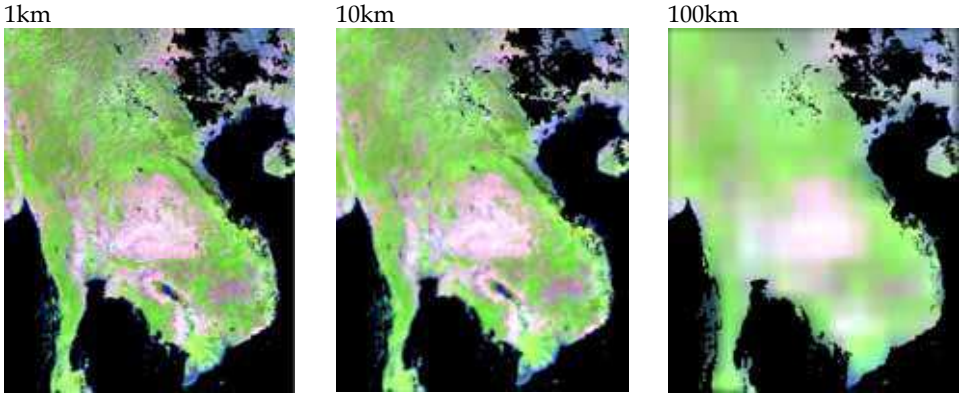

Fig. 3. Examples of original finer (1km) and corresponding simulated coarser images (10km and 100km).

3.2 Results

Two different situations are considered in this application. In the first situation, one assumes that the finer resolution images are exhaustively known for the previous year. Consequently, one can choose the most relevant previous finer image. In the second situation, one assumes that there is only one previous finer resolution image, so that there may be a seasonal shift between the previous and the objective finer resolution images (see Fig. 2 for the differences between seasons). Both situations are described and compared hereafter in the next subsections.

3.2.1 Situation 1: finer resolution images exhaustively known for the previous year

The methodology of Section 2.2 was applied here in the case where finer resolution images are exhaustivelly known for the previous year and when using coarser resolution input images either at 10km or at 100km (Fig. 4). Using the finer resolution image one year before the target date (i.e. at the same biweekly composite number but at the previous year) is a relevant choice for the finer resolution input in the fusion method : in that case, the previous finer resolution image and the new objective image correspond to the same period. As a consequence, there will be less changes due to the seasonal shift between both finer images.
Fig. 5 shows the evolution of the fused image for the year 2005 when using 100km coarser images. By comparison with the true evolution of the 1km images in Fig. 2, there is no significant color difference between the predicted images from the BDF method and the objective images. Futhermore, it is clear that the details from the finer resolution images are correctly accounted for in the fused images while the colors are updated by the coarser images (Fig. 6 illustrates this for the 21st biweekly composite image and with 100km coarser image). Results (not shown here) were also convincing with the 10km coarser input images.
It is also worth noting that, although only one finer image was chosen in this application for sake of brevity, there is no theoretical limitation on the number of finer resolution images to be accounted for within the BDF framework. The methodology presented in Section 2.2 and

more specifically Eqs. 4 and 5 can easily be generalized to the case of multiple finer resolution input images with no additional theoretical development. It is thus possible to account for the entire time series of the finer resolution images (before and after the objective image) . This is left for further researches at this point.

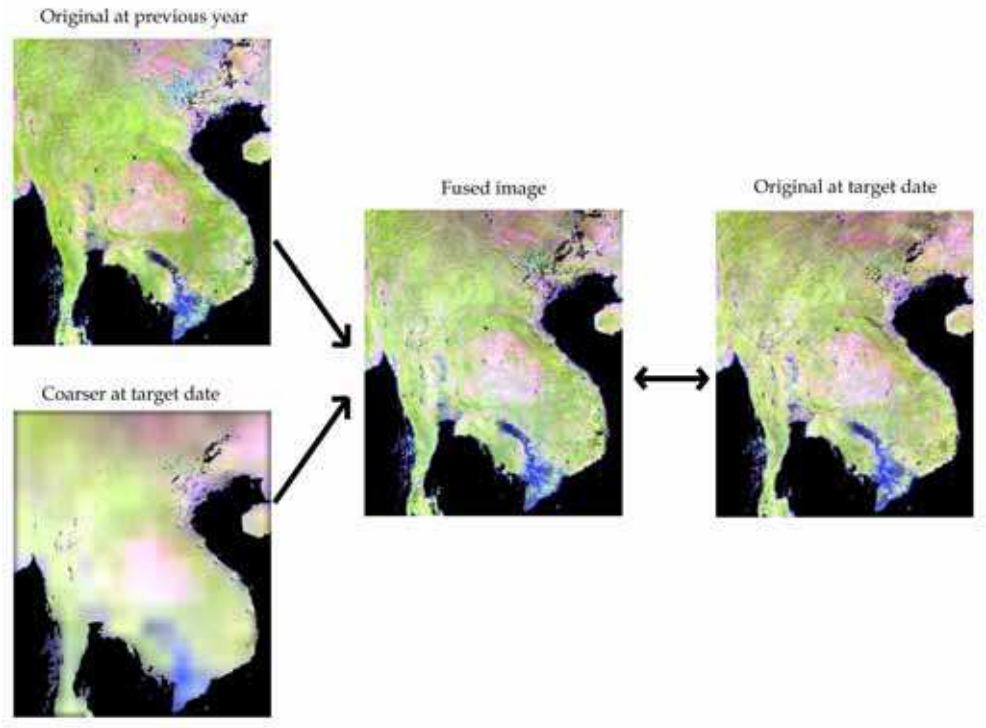

Fig. 4. Situation 1. Inputs for the fusion are the original 1km image at previous year and the coarser image (here 100km) at the target date. Fused images are then compared with the true original 1km images at the target date.

3.2.2 Situation 2: finer resolution image known for only one previous date

In the second situation, the finer resolution input image is assumed to be available at only one biweekly composite image. By doing this, the previous situation is thus generalized to the case where there is less available information at the finer resolution. The past finer image can be located anywhere in the current year (or even be related to a previous year) so that the seasonal effects are not necessarily seen in the finer image. Furthermore, the information relevance of the finer image with respect to the fused one is expected to drop along with the change of seasons (e.g. rainy season *versus* dry saison). As a consequence, the seasonal trend will only be included by the coarser image and details from the finer image will be included as long as the past and target biweekly images will correspond to the same season. In order to illustrate this situation, the only finer resolution image was assumed to be the first 1km biweekly image of the year 2005. Fig. 7 illustrates this situation in the case of 10km coarser images, although the methodology is of course the same for 100km.

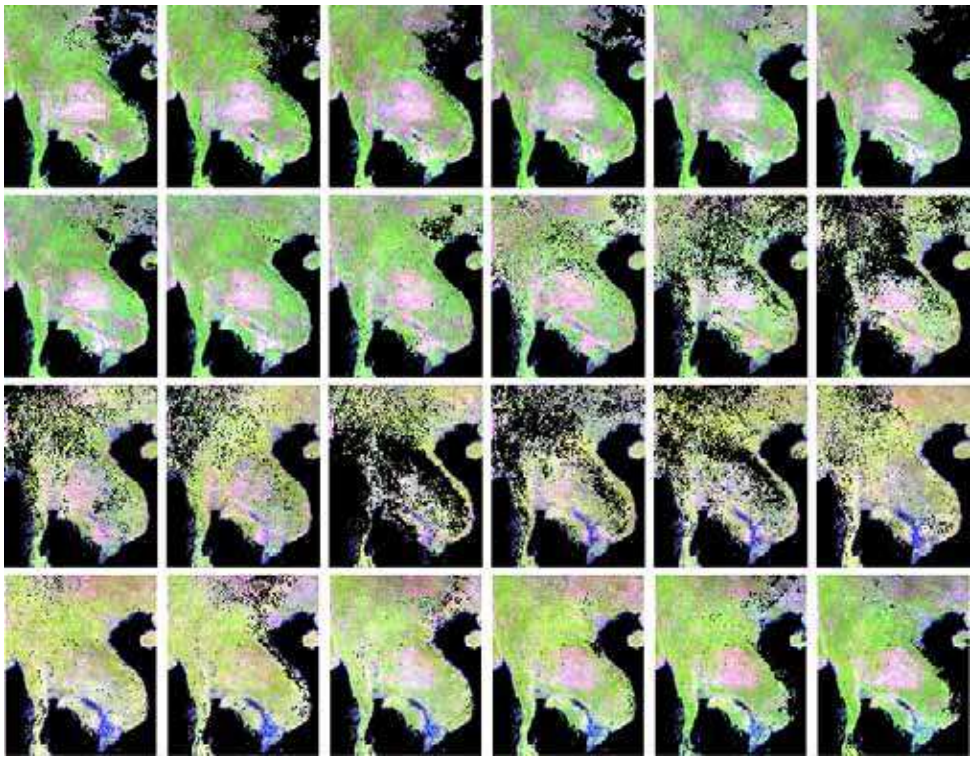

Fig. 5. Evolution of the decadal fused images for year 2005 when using the biweekly composite high spatial resolution image of the previous year. The resolution of the coarser images is equal to 100km here.

Similarly to the previous situation, the same methodology was applied for both spatial resolution for the coarser image (10km and 100km). Fig. 8 shows the temporal evolution of the fused images when using 10km coarser images. Again, a simple comparison between Figs. 2 and 8 shows that this temporal evolutation is in good accordance with the temporal evolution of the target images at 1km resolution (it is worth noting that pixels that were covered by clouds in the finer input image were of course not updated in the fused images). Furthermore, Fig. 9 illustrates the effect of the inputs on the fused results. Indeed, one can clearly see that the change of colors between the first and the second dates is correctly accounted for thanks to the 10km coarser image while the details from the previous finer resolution image are well preserved. Results (not shown here) were also in good accordance when using the 100km coarser images.

3.2.3 Quality assessment and comparison between both situations

Several indices were chosen for the quality assessment of the fused images. As time series are complete for each of the three spatial resolution, it is straightforward to compare updated images with the true images at 1km at each of the 25 biweekly period of year 2005. More specifically, one can compute the Mean Error (ME), the Mean Absolute Error (MAE) and the Root Mean Squared Error (RMSE) with

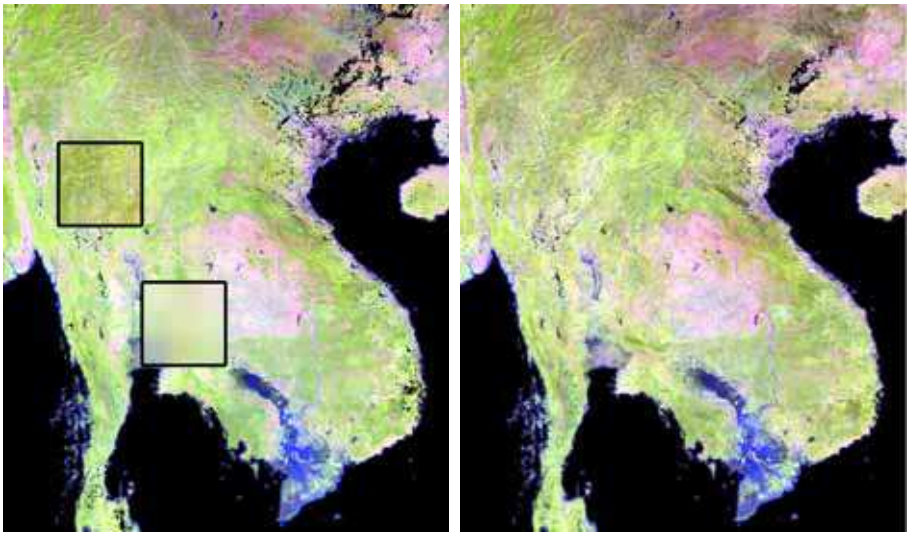

Fig. 6. On the left : the 21st biweekly fused image when using (i) original 1km image at previous year (upper rectangle) and (ii) coarser 100km image at target date (lower rectangle). On the right : original 21st biweekly 1km image.

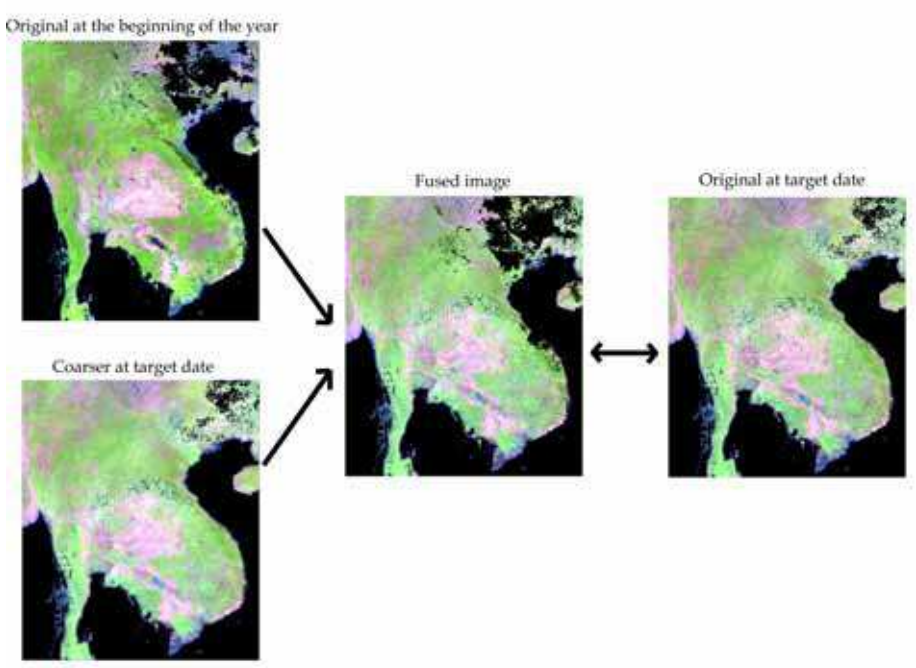

Fig. 7. Situation 2. Inputs for the fusion are the first biweekly original 1km image of the year and the coarser image (here 10km) at the target date. Fused images are then compared with the true original 1km images at the target date.

$$ME = \frac{1}{N}\sum_{k=1}^{N} E_k \tag{6}$$

$$MAE = \frac{1}{N}\sum_{k=1}^{N} | E_k | \tag{7}$$

$$RMSE = \sqrt{\frac{1}{N}\sum_{k=1}^{N} E_k^2} \tag{8}$$

where E_k is the difference between pixels values of the true and the fused images and N is the number of pixels in the images. It is worth noting that these indices were computed without cloud pixels (i.e. pixels that are detected as clouds at least once in the two images).
Fig. 10 shows the evolution of the ME for Situations 1 and 2, both for the two coarser resolution (each curve corresponds to a different spectral band). It is clear from these results that using the finer image of the previous year and the 10km coarser image provides the best results regarding the ME, while the ME values have larger amplitudes in the other cases (especially in the case of only one finer image and 100km coarser image). However, these amplitudes are significantly small (reflectance values belong to [0,1] interval) in order to conclude that the method is unbiased.

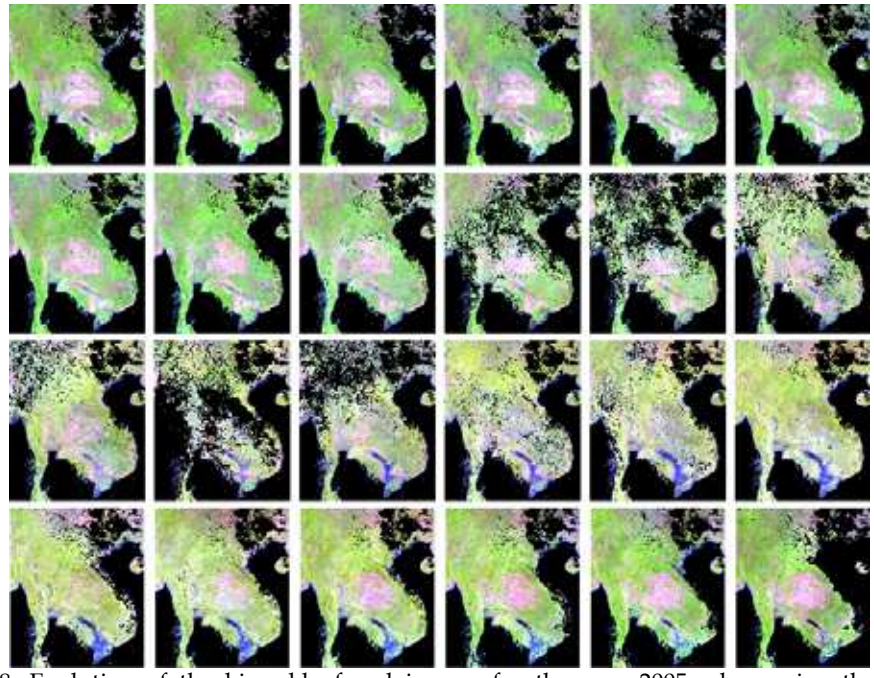

Fig. 8. Evolution of the biweekly fused images for the year 2005 when using the first biweekly finer image of the current year. The resolution of the coarser images was equal to 10km here.

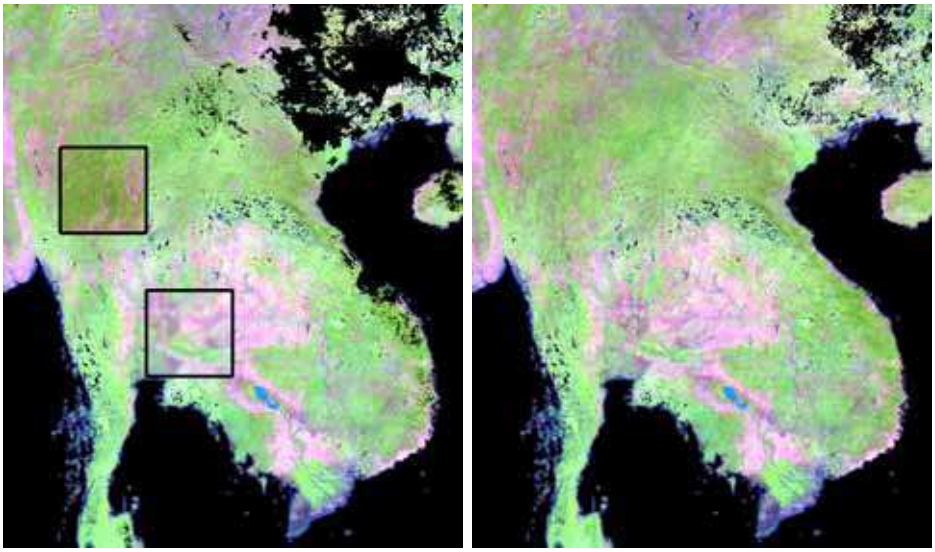

Fig. 9. On the left : the 9th biweekly fused image when using (i) original 1km image at beginning of the year (upper rectangle) and (ii) coarser 10km image at target date (lower rectangle). On the right : original 9th biweekly 1km image.

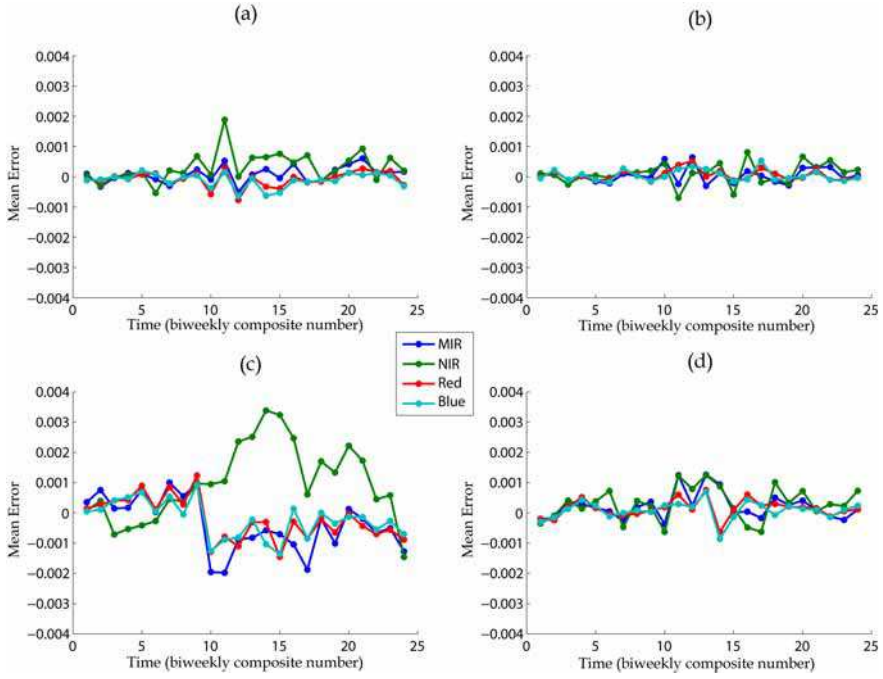

Fig. 10. Evolution of the Mean Error (reflectance) as a function of the time for Situations 1 (b and d) and 2 (a and c), both for the 10km (a and b) and the 100km (c and d) coarser resolutions.

Similarly, Figs. 11 and 12 show respectively the evolutions of the MAE and RMSE for the various cases. Again, it is clear from these results that it is preferable to use the finer resolution image of the previous year than to rely on a unique finer image at another season. However, the MAE and RMSE significantly increase between the 10th and the 20th biweekly composite numbers (i.e. the end of the dry season and the beginning of the rain season). Therefore, fused images are less precise for this period of the year. This is probably a consequence of both the intra and inter annual variation of the vegetation in the studied area.

As there were two secondary information sources (i.e. the past finer image and the coarser one at target date), it is also interesting to focus on the influence of these sources on the fused images. For this, correlation coefficients were computed between corresponding spectral bands of the different images. Again, these coeficients were computed at each biweekly composite number, allowing us to see how they evolve over time.

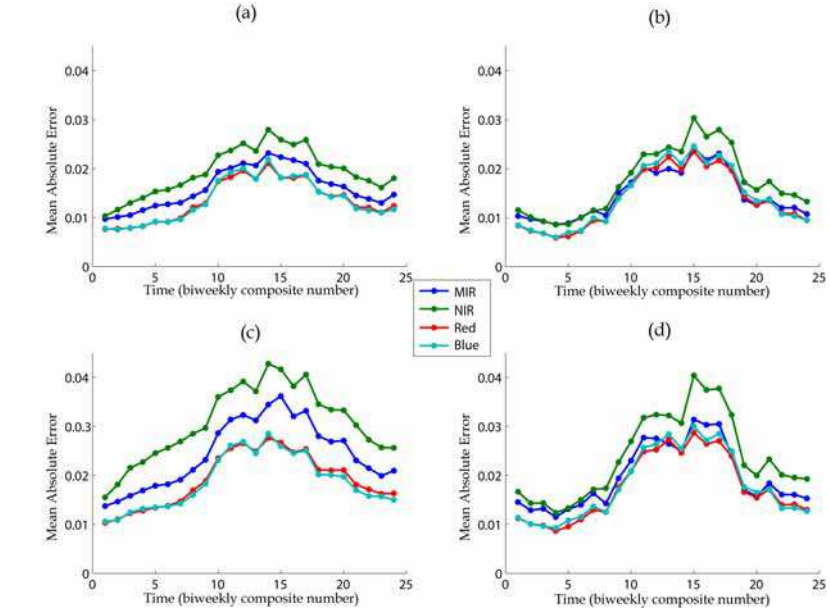

Fig. 11. Evolution of the Mean Absolute Error (reflectance) as a function of the time for Situations 1 (b and d) and 2 (a and c), both for the 10km (a and b) and the 100km (c and d) coarser resolutions.

Correlation coefficients between the fused and the original 1km input images are represented in Fig. 13. It is worth noting that the influence of the finer resolution image decreases rapidly at the end of the first quarter of the year (i.e. end of the dry season) when using the finer resolution image at the first biweekly compsite, whereas this influence remains rather constant when using the finer image of the previous year. This is of course

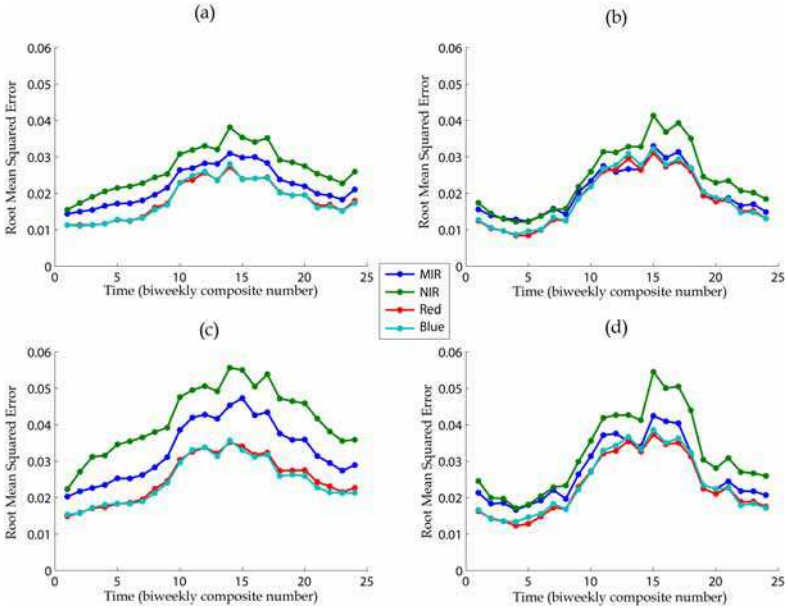

Fig. 12. Evolution of the Root Mean Squared Error (reflectance) as a function of the time for Situations 1 (b and d) and 2 (a and c), both for the 10km (a and b) and the 100km (c and d) coarser resolutions.

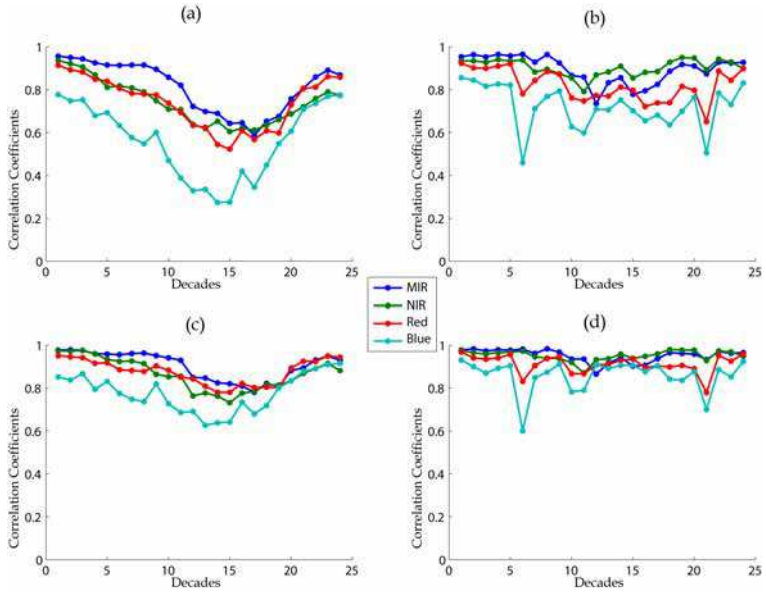

Fig. 13. Evolution of the correlation coefficients between fused and original 1km input images as a function of the time for Situations 1 (b and d) and 2 (a and c), both for the 10km (a and b) and the 100km (c and d) coarser resolutions.

mainly due to the fact that there is a significant seasonal shift of vegetation between the first biweekly composite of the year (i.e. beginning of the dry season) and the middle of the year (i.e. rainy season). Furthermore, the correlation coefficients increase significantly during the rainy season, i.e. when the vegetation starts to grow again. It is also worth noting that the influence of the finer input image on the fusion results is bigger when using 100km coarser image. This is simply because 10km images are more relevant for the prediction at 1km than 100km ones. Thus, as 100km images are less informative, their influence on the fused images is smaller.

Similarly, it is interesting to focus on the evolution of the coarser images's influences on the fused results (Fig. 14). It is worth noting that this influence is rather constant when using the first biweekly finer image of the current year, while it drops in the middle of the year when using the finer image of the previous year. These behaviors are thus precisely opposite with those observed for the finer resolution images in Fig. 13. Again, it is mainly due to the fact that the finer images of the previous year correspond to the same season as the target unknown image, thus globally exhibiting the same vegetation conditions. As a consequence, fused images rely a little bit less on the coarser image for the update of the previous finer images (i.e. correlation coefficients are smaller).

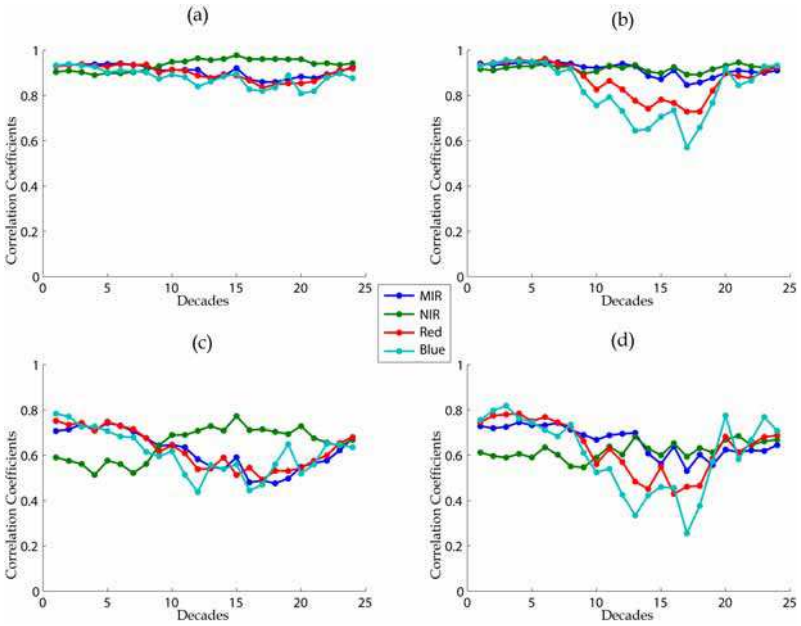

Fig. 14. Evolution of the correlation coefficients between fused and coarser input images as a function of the time for Situations 1 (b and d) and 2 (a and c), both for the 10km (a and b) and the 100km (c and d) coarser resolutions.

4. Conclusion

In this chapter, a Bayesian data fusion (BDF; Bogaert & Fasbender, 2007) framework was applied for the update of scare high resolution images with time series of coarser images. This BDF framework aims at reconciling various secondary information sources into a unique prediction. Although initially proposed in a spatial prediction context, a generalization of this BDF approach was presented here for space-time predictions. It is worth noting that, as information are known exhaustively over space, the use of remotely sensed images is a singular case of secondary information sources so that interpolation (or spatial predictions) is not even needed here. Other applications using this BDF framework can be found in (Fasbender et al., 2008a; Fasbender et al., 2008b; Fasbender et al., 2008c).

After a brief general description of the BDF framework, several specific hypotheses were assumed in order to account for the three available information sources (the coarser images at date 1 and 2 and the finer image at date 1). Based on these three images, two methods were considered for the prediction of the target image (i.e. the finer image at date 2). The first method was to consider the coarser image at date 2 as a raw estimation of the target image. The second method was based on a High-Pass Filter (HPF) approach for which the lower frequencies of the finer image at date 1 are substituted by the coarser image at date 2. Consequently, details are provided by the high resolution image at date 1 whereas the global fluctuations are provided by the coarser image at date 2. The final prediction is eventually based on the combination of both methods within the BDF framework.

In this chapter, the proposed methodology was applied to a synthetic case study. Coarser images were simulated from biweekly composite images based on real 1km SPOT VEGETATION images in the South-East Asia region. Two coarser resolutions were tested here : 10km and 100km (even if the ratio between finer and coarser resolution images is expected to be smaller for real case applications). Moreover, two situations differing with respect to the amount of information sources at finer resolution were considered in this illustration. In Situation 1, finer resolution images were assumed to be available for the whole previous year, whereas only one finer image was available in Situation 2 (here, the first biweekly image of year 2005). Results showed that the method correctly accounted for the important seasonal trend due to the dry and rain seasons whatever the resolution of the coarser images (10km or 100km) or the amount of available finer images (only one or the whole previous year). Although visual interpretations were clearly in favor of BDF predictions, a validation was also performed using the true 1km images. Mean Error (ME), Mean Absolute Error (MAE) and Root Mean Squared Error (RMSE) were computed for each spectral band, both situations and both coarser resolutions, as a function of the time. Although the ME values fluctuate around zero (showing the accuracy of the method), the MAE and the RMSE values increase during the dry season (showing thus that there is a drop of precision for the method in this period of the year). This effect is most probably due to local changes of vegetation that are not observable at the coarser resolutions. However, results showed that using the finer image of previous year and 10km coarser images led to the most efficient updates (i.e. smaller ME, MAE and RMSE amplitudes).

As there were two methods of prediction to be merged within the BDF framework, it is also intersting to focus on their respective influences on the fused images. Results showed that the influence of the finer input images is rather constant in Situation 1, while this influence drops during the dry season in Situation 2. This is of course mainly due to the fact that, in Situation 1, finer input images and target ones are assumed to correspond to the same season, exhibiting thus the same stage of vegetation. Conversly, the influence of the coarser images on the fused images drops during the dry season in Situation 1, while being rather constant in Situation 2. Again, this inversion is probably due to the fact that the finer input and the target images are more similar in Situation 1 than in Situation 2, thus relying less on the coarser input image in Situation 1.

Although we only applied it here to a synthetic case study, generalizations of this BDF method are possible in order to tackle real case applications. As examples, using finer and coarser images with different spectral bands and using more than one past finer images for the prediction are just two possibilities for future researches. It thus opens new avenues in the context of updating high resolution images with coarser images.

5. Acknowledgment

The authors would like to thanks the Belgian Scientific Policy for funding the DYNMAP project through the STEREO II earth observation program.

6. References

Aiazzi, B.; Alparone, L.; Baronti, S. & Garzelli, A. (2002). Context-driven fusion of high spatial and spectral resolution images based on oversampled multiresolution analysis, *IEEE Trans. Geosci. Remote Sens.*, Vol. 40, No. 10, October 2002, 2300-2312.

Ballester, C.; Caselles, V.; Igual, L.; Verdera, J. & Rougé, B. (2006). A variational model for P+XS image fusion, *Int. J. Comput. Vision*, Vol. 69, No. 1, August 2006, 43-58.

Bogaert, P. & Fasbender, D. (2007). Bayesian data fusion in a spatial prediction context : a general formulation, *Stoch. Env. Res. Risk A.*, Vol. 21, No. 6, November 2007, 695-709, ISSN 1436-3240.

Bruzzone, L.; Cossu, R. & Vernazza, G. (2002). Combining parametric and non-parametric algorithms for a partially unsupervised classification of multitemporal remote-sensing images, *Inf. Fusion*, Vol. 3, No. 4, December 2002, 289-297.

Chavez, P. S.; Sides, S. C. & Anderson, A. (1991). Comparison of three diffrent methods to merge multiresolution and multispectral data: Landsat TM and SPOT panchromatic. *Photogram. Eng. Remote Sens.*, Vol. 57, No. 3, June 1991, 295-303.

Chung, A. C. S. & Shen, H. C. (2000). Entropy-based Markov chains for multisensor fusion, *J. Intell. Robot. Syst.*, Vol. 29, No. 2, October 2000, 161-189.

Fasbender, D.; Peeters, L.; Bogaert, P. & Dassargues, A. (2008a). Bayesian data fusion applied to water table spatial mapping, *Water Resour. Res.*, Vol. 44, W12422,doi:10.1029/2008WR006921

Fasbender, D.; Radoux, J. & Bogaert, P. (2008b). Bayesian data fusion for adaptable image pansharpening, *IEEE Trans. Geosci. Remote Sens.*,Vol. 46, No. 6, June 2008, 1847-1857, ISSN 0196-2892.

Fasbender, D.; Tuia, D.; Bogaert, P. & Kanevski, M. (2008c). Support-based implementation of Bayesian data fusion for spatial enhancement: Application to ASTER thermal images, *IEEE Geosci. Remote Sens. Letters*, Vol. 5, No. 4, October 2008, 598-602, ISSN 1545-598X.

Garzelli, A. & Nencini, F. (2005). Interband structure modeling for Pan-sharpening of very high-resolution multispectral images, *Inf. Fusion*, Vol. 6, No. 3, September 2005, 213-224.

Harrison, B. A. & Jupp, D. L. B. (1990). *Introduction to image processing*, CSIRO Division of Water Resources, ISBN 978-0643051089, Canberra.

Jones, G. D.; Allsop, R. E. & Gilby, J. H. (2003). Bayesian analysis for fusion of data from disparate imaging systems for surveillance, *Image and Vision Computing*, Vol. 21, No. 10, September 2003, 843-849.

Laporterie-Déjean, F.; de Boissezon, H.; Flouzat, G. & Lefèvre-Fonollosa, M.-J. (2005). Thematic and statistical evaluations of five panchromatic/multispectral fusion methods on simulated PLEIADES-HR images, *Inf. Fusion*, Vol. 6, No. 3, September 2005, 193-212.

Mitchell, H.B. (2007). *Multi-Sensor Data Fusion,* Springer-Verlag, ISBN 978-3-540-71463-7, Berlin Heidelberg.

Moshiri, B.; Asharif, M. R. & Hosein Nezhad, R. (2002). Pseudo information measure: a new concept for extension of Bayesian fusion in robotic map building, *Inf. Fusion*, Vol. 3, No. 1, March 2002, 51-68.

Pardo-Iguzquiza, C.; Chica-Olmo, M. & Atkinson, P. M. (2006). Downscaling cokriging for image pansharpening, *Remote Sens. Environ.*, Vol. 102, No. 1-2, May 2006, 86-98.

Pinheiro, P. & Lima, P. (2004). Bayesian Sensor Fusion for Cooperative Object Localization and World Modeling, *Proceedings of the 8th Conference on Intelligent Autonomous Systems, IAS-8*, Amsterdam, The Netherlands.

Pohl, C. & van Genderen, J. L. (1998). Multisensor image fusion in remote sensing : concepts, methods and applications, *Int. J. Remote Sens.*, Vol. 19, No. 5, March 1998, 823-854.

Rajan, D. & Chaudhuri, S. (2002), Data fusion techniques for super-resolution imaging, *Inf. Fusion*, Vol. 3, No. 1, March 2002, 25-38.

Ranchin, T.; Aiazzi, B.; Alparone, L.; Baronti, S. & Wald, L. (2003). Image fusion - the ARSIS concept and some successful implementation schemes, *ISPRS J. Photogram. Remote Sens.*, Vol. 58, No. 1-2, June 2003, 4-18.

Vancutsem, C.; Pekel, J.F.; Bogaert, P. & Defourny, P. (2007). Mean compositing, an alternative strategy for producing temporal syntheses. Concepts and perfomance assessment for SPOT VEGETATION time series. *Int. J. Remote Sens.*, Vol. 28, No. 22, November 2007, 5123-5141.

Wang, Z.; Ziou, D.; Armenakis, C.; Li, D. & Li, Q. (2005). A comparative analysis of image fusion methods, *IEEE Trans. Geosci. Remote Sens.*, Vol. 43, No. 6, June 2005, 1391-1402.

Wikle, C. K.; Milliff, R. F.; Nychka, D. & Berliner, L. M. (2001). Spatial-temporal hierarchical Bayesian modeling: Tropical ocean surface winds, *J. Am. Stat. Assoc.*, Vol. 96, No. 454, June 2001, 382-397, ISSN 0162-1459.

Zhou, J.; Civco, D. L. & Silander, J. A. (1998). A wavelet transform method to merge Landsat TM and SPOT panchromatic data, *Int. J. Remote Sens.*, Vol. 19, No. 4, March 1998, 743-757.

Sensor and Data Fusion

Edited by Nada Milisavljevic

ISBN 978-3-902613-52-3
Hard cover, 436 pages
Publisher I-Tech Education and Publishing
Published online 01, February, 2009
Published in print edition February, 2009

Data fusion is a research area that is growing rapidly due to the fact that it provides means for combining pieces of information coming from different sources/sensors, resulting in ameliorated overall system performance (improved decision making, increased detection capabilities, diminished number of false alarms, improved reliability in various situations at hand) with respect to separate sensors/sources. Different data fusion methods have been developed in order to optimize the overall system output in a variety of applications for which data fusion might be useful: security (humanitarian, military), medical diagnosis, environmental monitoring, remote sensing, robotics, etc.

How to reference

In order to correctly reference this scholarly work, feel free to copy and paste the following:

Dominique Fasbender, Valérie Obsomer, Patrick Bogaert and Pierre Defourny (2009). Updating Scarce High Resolution Images with Time Series of Coarser Images: a Bayesian Data Fusion Solution, Sensor and Data Fusion, Nada Milisavljevic (Ed.), ISBN: 978-3-902613-52-3, InTech, Available from: http://www.intechopen.com/books/sensor_and_data_fusion/updating_scarce_high_resolution_images_with_time_series_of_coarser_images__a_bayesian_data_fusion_so

INTECH
open science | open minds

InTech Europe
University Campus STeP Ri
Slavka Krautzeka 83/A
51000 Rijeka, Croatia
Phone: +385 (51) 770 447
Fax: +385 (51) 686 166
www.intechopen.com

InTech China
Unit 405, Office Block, Hotel Equatorial Shanghai
No.65, Yan An Road (West), Shanghai, 200040, China
中国上海市延安西路65号上海国际贵都大饭店办公楼405单元
Phone: +86-21-62489820
Fax: +86-21-62489821